Key Features for Designing Phosphodiesterase-5 Inhibitors

http://www.jbsdonline.com

Abstract

Phosphodiesterase superfamily is the key regulator of 3',5'-cyclic guanosine monophosphate (cGMP) decomposition in human body. Phosphodiesterase-5 (PDE-5) inhibitors, sildenafil, vardenafil and tadalafil, are well known oral treatment for males with erectile dysfunction. To investigate the inhibitory effects of traditional Chinese medicine (TCM) compounds to PDE-5, we performed both ligand-based and structure-based studies on this topic. Comparative molecular field analysis (CoMFA) and comparative molecular similarity indices analysis (CoMSIA) studies were conducted to construct three dimensional quantitative structure-activity relationship (3D-QSAR) models of series of known PDE-5 inhibitors. The predictive models had cross-validated, q^2, and non cross-validated coefficient, r^2, values of 0.791 and 0.948 for CoMFA and 0.724 and 0.908 for CoMSIA. These two 3D-QSAR models were used to predict activity of TCM compounds. Docking simulations were performed to further analyze the binding mode of training set and TCM compounds. A putative binding model was proposed based on CoMFA and CoMSIA contour maps and docking simulations; formation of pi-stacking, water bridge and specific hydrogen bonding were deemed important interactions between ligands and PDE-5. Of our TCM compounds, engeletin, satisfied our binding model, and hence, emerged as PDE-5 inhibitor candidate.

Using this study as an example, we demonstrated that docking should be conducted for qualitative purposes, such as identifying protein characteristics, rather than for quantitative analyses that rank compound efficacy based on results of scoring functions. Prediction of compound activity should be reserved for QSAR analyses, and scoring functions and docking scores should be used for preliminary screening of TCM database (http://tcm.cmu.edu.tw/index.php).

Key words: Phosphodiesterase-5; Nitric oxide; Comparative molecular field analysis (CoMFA); Comparative molecular similarity indices analysis (CoMSIA); Docking; Traditional Chinese medicine (TCM).

Introduction

Penile erection is a physiological response mediated by complex biochemical signaling mechanism in which nitric oxide (NO) is emerging as the central component of the process (1). This molecule could stimulate soluble guanylate cyclase that converts guanosine triphosphate (GTP) to second messenger, 3',5'-cyclic guanosine monophosphate (cGMP), which could relax smooth muscle and leads to vasodilatation (2). Thus, the release of NO from neural and endothelial components of the penile corporal body could increase blood flow to *corpora cavernosa*, leading to erection.

Phosphodiesterase superfamily is the key enzyme for degrading the intracellular cGMP (3, 4). This superfamily of enzymes is a well studied drug target involved in treatment of many diseases, including heart failure, depression, asthma, and

Tung-Ti Chang[a,b]
Hung-Jin Huang[a]
Kuei-Jen Lee[c]
Hsin Wei Yu[a]
Hsin-Yi Chen[a]
Fuu-Jen Tsai[c,d]
Mao-Feng Sun[a,e]*
Calvin Yu-Chian Chen[a,c,f]*

[a]Laboratory of Computational and Systems Biology, School of Chinese Medicine, China Medical University, Taichung, 40402, Taiwan, ROC
[b]Department of Chinese Pediatrics, China Medical University Hospital, Taiwan, ROC
[c]Department of Bioinformatics, Asia University, Taichung, 41354, Taiwan, ROC
[d]Department of Medical Genetics, Pediatrics and Medical Research, China Medical University Hospital and College of Chinese Medicine, China Medical University, Taichung, 40402, Taiwan, ROC
[e]Department of Acupuncture, China Medical University Hospital, Taiwan, ROC
[f]Computational and Systems Biology, Massachusetts Institute of Technology, Cambridge, MA 02139, USA

*Phone: +1-617-353-7123
E-mail: ycc@mail.cmu.edu.tw
ycc929@MIT.EDU (C.Y.-C. Chen)

inflammation (5-9). Phosphodiesterase-5, in particular, is most well known for being the target of sildenafil (Viagra) and tadalafil (Cialis) that are often used to treat erectile dysfunction. However, these two PDE-5 inhibitors are not without physiological side effects. Non-specific interaction of these inhibitors to PDE-6 or PDE-11 could cause headache and optical interruption (10-12).

In previous researches, natural compounds isolated have been shown to possess therapeutic potentials (13-15). To investigate the potential inhibitory effects of traditional Chinese medicine (TCM) compounds to PDE-5, we employed computation approaches, which are widely employed now for designing new therapeutics (16-19), to analyzed compounds from our TCM database (http://tcm.cmu.edu.tw/index.php). We constructed comparative molecular field analysis (CoMFA) and comparative molecular similarity indices analysis (CoMSIA) model based on tested PDE-5 inhibitors, and used the models for predicting the activity of TCM products. Docking simulations were also performed to investigate the binding mode of cGMP, sildenafil, training set and TCM candidates. In our past experiences, both structure-based methods and ligand-based methods could be used for drug design (20-23). Three dimensional structure-activity relationships (3D-QSAR) could point out major molecular properties of ligands (23), and structure-based studies, on the other hand, could analyze specific ligand-protein interactions in molecular dynamics simulations (24-29), protein structure analyses (30-34) and docking simulations (35-37).

Methodology

Data Set

The training set and the test set used for CoMFA and CoMSIA analyses were taken from previous researches (38-46) that have experimentally tested and measured compound IC_{50}. Structures of compounds in the training set (56) and the test set (29) are shown in Table I.

Three-dimensional structure building of the training set, test set and TCM compounds were first drawn in two-dimension using ChemBioDraw Ultra 11.0 (CambridgeSoft Inc., USA) and then transformed to three-dimension using ChemBio3D Ultra 11.0 (CambridgeSoft Inc., USA). Energy minimizations were performed using the MM2 force field available in the CambridgeSoft ChemBio3D package.

Molecular Modeling

CoMFA and CoMSIA QSAR analyses were conducted using SYBYL 8.0 package (Tripos Inc., St. Louis, MO, USA). The initial alignment of the training set (a requirement prior to CoMFA and CoMSIA studies) was obtained using the SYBYL atom-fit alignment feature. The core atoms used from alignment is shown in Figure 1 (a).
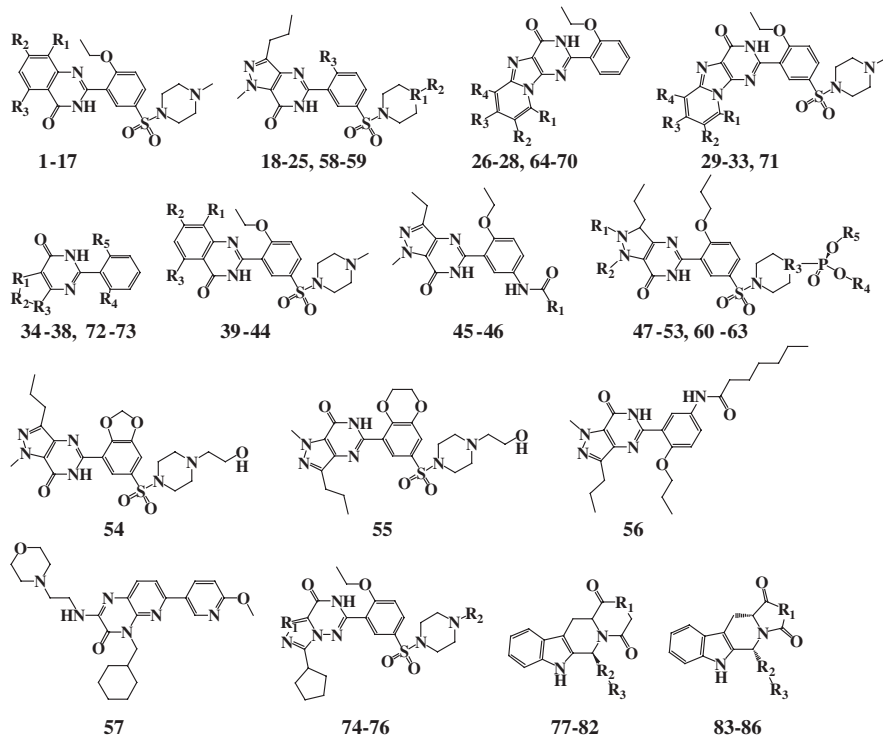
CoMFA and CoMSIA Model

In building the CoMFA model, the SYBYL default energy setting was used, and the two physicochemical properties computed, steric and electrostatic energies, were described by Lennard-Jones potentials and Coulomb potentials, respectively. As for the CoMSIA model, the energy cutoff setting was the same as CoMFA, and three property fields, namely hydrophobic, hydrogen bond acceptor and hydrogen bond donor, were evaluated in addition to steric and electrostatic properties.

The correlation between the property descriptors and biological activities, pIC_{50}, was analyzed in partial least square (PLS) method. The predictive models built from the PLS analyses were tested in leave-one-out (LOO) cross validation. The cross-validated coefficient, q^2, as well as the non cross-validated coefficient, r^2, and standard error of estimate were computed.

Table I
Structure of compounds in training set and test set.

1-17   **18-25, 58-59**   **26-28, 64-70**   **29-33, 71**

34-38, 72-73   **39-44**   **45-46**   **47-53, 60-63**

54   **55**   **56**

57   **74-76**   **77-82**   **83-86**

Compound	R_1	R_2	R_3	R_4	R_5	pIC_{50}
Training Set						
1	F	OCH_3	OCH_3	-	-	8.54
2	Cl	OCH_3	OCH_3	-	-	7.44
3	Br	OCH_3	OCH_3	-	-	7.47
4	I	OCH_3	OCH_3	-	-	7.84
5	-	OCH_3	OCH_3	-	-	8.64
6	CH_3	OCH_3	OCH_3	-	-	8.62
7	C_2H_5	OCH_3	OCH_3	-	-	7.57
8	C_2H_3	OCH_3	OCH_3	-	-	6.27
9	C_5H_{11}	OCH_3	OCH_3	-	-	8.22
10	F	OCH_3	OH	-	-	8.15
11	I	OCH_3	OH	-	-	7.21
12	-	OCH_3	OH	-	-	7.51
13	CH_3	OCH_3	OH	-	-	7.70
14	C_2H_5	OCH_3	OH	-	-	7.35
15	C_2H_3	OCH_3	OH	-	-	7.21
16	C_4H_9	OCH_3	OH	-	-	6.44
17	C_5H_{11}	OCH_3	OH	-	-	7.54
18	CH	COOH	OCH_2CH_3	-	-	5.08
19	CH	CH_2COOH	OCH_2CH_3	-	-	5.20
20	CH	$(CH_2)_3COOH$	OCH_2CH_3	-	-	5.09
21	CH	$(CH_2)_5COOH$	OCH_2CH_3	-	-	5.04
22	N	$(CH_2)_3COOH$	OCH_2CH_3	-	-	5.04
23	CH	COOH	$O(CH_2)_2CH_3$	-	-	5.02
24	CH	CH_2COOH	$O(CH_2)_2CH_3$	-	-	5.09
25	CH	$(CH_2)_3COOH$	$O(CH_2)_2CH_3$	-	-	5.13
26	CH_2CH_3	-	-	-	-	5.22
27	-	CN	-	-	-	5.22
28	CH_3	CN	-	-	-	5.19
29	-	-	-	-	-	5.16
30	-	-	-	CH_3	-	5.25
31	-	-	CH_3	-	-	5.21
32	-	CH_3	-	-	-	5.25

(Continued)

Table I *(Continued)*

Compound	R₁	R₂	R₃	R₄	R₅	pIC₅₀
33	CH_3	-	-	-	-	5.21
34	-	Br	-	-	-	5.26
35	NH	N	$C(CH_2)_2CH_3$	-	OCH_2CH_3	8.30
36	NCH_3	N	$C(CH_2)_2CH_3$	OCH_2CH_3	-	7.04
37	N	N	$N(CH_2)_2CH_3$	OCH_2CH_3	-	7.82
38	N	N	N-cyclopentane	OCH_2CH_3	-	7.59
39	O	N	C-cyclopentane	OCH_2CH_3	-	8.30
40	N	C	$N-(CH_2)_2CH_3$	-	-	7.39
41	$N(CH_2)_2CH_3$	N	$C-CH_3$	-	-	7.05
42	$N(CH_2)_2CH_3$	N	$C-CH_2CH_3$	-	-	7.52
43	CCH_2CH_3	N	N-cyclopentane	-	-	7.00
44	$C(CH_2)_2CH_3$	N	$N-CH_3$	-	-	7.22
45	$N-CH_3$	N	N-cyclopentane	-	-	8.10
46	$(CH_2)_2CH_3$	-	-	-	-	5.68
47	isopropyl	-	-	-	-	5.72
48	-	CH_3	NCH_2	H	-	6.32
49	CH_3	-	$N(CH_2)_3$	H	-	5.66
50	-	CH_3	CH	H	-	5.51
51	-	CH_3	$CHCH_2$	H	-	5.47
52	-₃	CH_3	NCH_2	CH_2CH_3	-	5.45
53	-	CH_3	$N-(CH_2)_3$	CH_2CH_3	-	5.46
54	-	-	-	-		5.40
55	-	-	-	-		5.37
56	-	-	-	-		6.16
Test Set						
57	N	$(CH_2)_2OH$	2,3-dihydrofuran	-	-	6.83
58	N	$(CH_2)_2OH$	3,4-dihydro-2H-pyran	-	-	5.47
59	-	CH_3	$CHCH_2$	CH_2CH_3	CH_2CH_3	5.42
60	-	CH_3	$N-(CH_2)_3$	H	H	5.47
61	-	CH_3	CH	H	H	5.46
62	-	CH_3	$CHCH_2$	H	H	5.45
63	-	-	-	CH_3	-	5.45
64	-	-	CH_3	-	-	5.42
65	-	CH_3	-	-	-	5.49
66	CH_3	-	-	-	-	5.53
67	-	Br	-	-	-	5.47
68	CH_3	Br			-	5.52
69	CH_3	Br	-	Br	-	5.50
70	CH_3	-		-	-	5.46
71	N	N	$(CH_2)_2CH_3$	-	-	5.15
72	N	N	C-cyclopentane	-	-	8.30
73	CCH_3	$(CH_2)_2OH$	-	-	-	7.92
74	CCH_2CH_3	CH_3	-	-	-	8.52
75	O	$(CH_2)_2OH$	-	-	-	8.10
76	NH	C_6H_5	1,3-dioxolane	-	-	7.30
77	NCH_3	C_6H_5	1,3-dioxolane	-	-	7.00
78	$N(CH_2)_3CH_3$	C_6H_5	-	-	-	7.30
79	$N(CH_2)_3CH_3$	C_6H_5	1,3-dioxolane	-	-	6.70
80	$N(CH_2)_3CH_3$	C_6H_{10}	Cl	-	-	7.30
81	NCH_3	C_6H_{10}	OCH_3	-	-	7.40
82	NCH_3	C_6H_5	1,3-dioxolane	-	-	6.52
83	$N(CH_2)_3CH_3$	pyridine	-	-	-	6.70
84	$N(CH_2)_3CH_3$	C_6H_5	Cl	-	-	6.86
85	$NCH_2C_6H_5$	C_6H_{10}	OCH_3	-	-	6.00

Docking Study

The LiangFit program of Accelrys Discovery Studio, version 2.5, was used to dock compounds into protein active site. LigandFit is a shape-directed docking method that generates ligand poses based on Monte Carlo conformational search and selects compounds most fitted to active site shape (47). We used this program to dock compounds of our TCM library into the PDE-5 cGMP binding site.
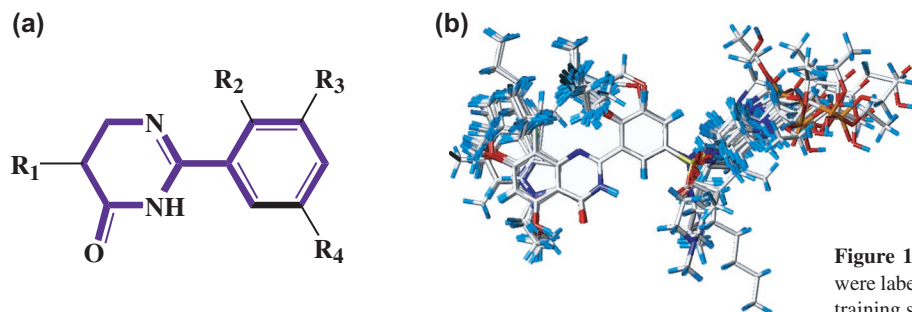
(a)

(b)

Figure 1: (**a**) Scaffold of training set and test set. Core atoms were labeled by bold face blue lines. (**b**) The atom-fit alignment of training set molecules.

The three-dimensional structure of PDE-5 was downloaded from the Protein Data Bank (PDB ID: IUDT) (48). Sildenafil citrate was cocrystallized with PDE-5, and its binding position was used to define ligand docking site. All water molecules in the protein crystal structure were retained in the docking simulations and remained immobile.

Chemistry at Harvard Macromolecular mechanics (CHARMm) forcefield (49) was applied to both protein and ligands prior to docking simulation steps. The maximum ligand poses retained after ligand-active site shape matching were set to 10. The Smart Minimizer option was used for final *in situ* ligand and protein minimization. There are 2000 steps taken for minimization.

Results and Discussion

QSAR by CoMFA and CoMSIA

As illustrated in Figure 1(a, b), the reference atoms used in the molecular alignment of the training set are set in bold face, and most structural differences of training set compound are found in R2, R3 and R4 positions.

The results of PLS analyses are shown in Tables II and III. The values of q^2 and r^2 were 0.791 and 0.948 for CoMFA. Hydrogen bond donor, hydrogen bond acceptor, steric and hydrophobic fields were taken into consideration for CoMSIA model, and the value of q^2 and r^2 were 0.724 and 0.908 for CoMFA. Table III also shows

Table II
PLS statistics of CoMFA model.

Parameters	Model
No. of training set compounds	56
No. of test set compounds	30
q^2	0.791
No. of components	6
r^2	0.948
SEE	0.296
F value	151.255
Steric region*	0.750
Electrostatic region*	0.250

* = the contribution of the region.
SEE = Standard Error of Estimate.

Table III
PLS statistics of CoMSIA model.

CoMSIA fields	q^2	Components	SEE	r^2	F value
A	0.603	4	0.556	0.809	56.243
D	0.775	6	0.424	0.893	71.222
H	0.579	5	0.490	0.855	61.347
E	0.044	6	1.248	0.077	0.712
S	0.686	5	0.516	0.839	54.342
D+A	0.740	4	0.460	0.870	88.395
D+H	0.717	5	0.434	0.886	80.958
D+E	0.712	6	0.451	0.880	62.072
D+S	0.747	4	0.463	0.868	87.177
D+H	0.735	5	0.433	0.887	81.293
D+S+A	0.729	6	0.433	0.889	67.835
D+S+H	0.699	4	0.452	0.874	92.075
D+S+E	0.716	6	0.436	0.887	66.812
D+S+A+H	0.724	6	0.393	0.908	84.155
D+S+A+E	0.728	5	0.450	0.878	74.747
A+D+H+E+S	0.735	6	0.415	0.898	74.883

SEE = Standard Error of Estimate.
A: Hydrogen bond acceptor regions; D: Hydrogen bond donor regions; H: Hydrophobic regions, E: Electrostatic regions; S: Steric regions.

Table IV
Activities of training set and test set predicted by CoMFA and CoMSIA.

Compound	pIC50	CoMFA Predict	residual (Δ)	CoMSIA Predict	residual (Δ)
1	8.540	8.140	0.400	8.337	0.203
2	7.440	7.724	-0.284	7.769	-0.329
3	7.470	7.711	-0.241	7.676	-0.206
4	7.840	7.713	0.127	7.555	0.285
5	8.640	8.188	0.452	8.554	0.086
6	8.620	8.246	0.374	8.315	0.305
7	7.570	7.297	0.273	7.157	0.413
8	6.270	6.849	-0.579	6.938	-0.668
9	8.220	7.905	0.315	7.895	0.325
10	8.150	7.916	0.234	8.051	0.099
11	7.210	7.404	-0.194	6.905	0.305
12	7.510	7.768	-0.258	7.952	-0.442
13	7.700	8.093	-0.393	8.041	-0.341
14	7.350	7.300	0.050	7.600	-0.250
15	7.210	7.035	0.175	6.820	0.390
16	6.440	7.026	-0.586	7.102	-0.662
17	7.540	7.333	0.207	7.044	0.496
18	5.080	5.483	-0.403	5.048	0.032
19	5.200	5.390	-0.190	5.33	-0.130
20	5.090	4.928	0.162	4.867	0.223
21	5.040	4.908	0.132	4.997	0.043
22	5.040	4.628	0.412	5.132	-0.092
23	5.020	4.758	0.262	5.026	-0.006
24	5.090	5.237	-0.147	5.411	-0.321
25	5.130	4.862	0.268	4.968	0.162
26	5.40	5.415	-0.015	5.322	0.078
27	5.370	5.073	0.297	5.313	0.057
28	6.430	6.295	0.135	6.376	0.054
29	5.680	5.636	0.044	5.808	-0.128
30	6.160	6.105	0.055	6.031	0.129
31	5.720	5.753	-0.033	5.876	-0.156
32	6.320	6.185	0.135	6.190	0.130
33	5.660	5.576	0.084	5.786	-0.126
34	5.510	5.522	-0.012	5.768	-0.258
35	5.470	5.606	-0.136	5.302	0.168
36	5.450	5.568	-0.118	5.389	0.061
37	5.460	5.428	0.032	5.398	0.062
38	5.220	5.437	-0.217	5.381	-0.161
39	5.220	5.011	0.209	5.254	-0.034
40	5.190	5.211	-0.021	5.269	-0.079
41	5.160	5.442	-0.282	5.364	-0.204
42	5.250	5.147	0.103	5.28	-0.030
43	5.210	5.405	-0.195	5.376	-0.166
44	5.250	5.307	-0.057	5.144	0.106
45	5.210	5.508	-0.298	5.029	0.181
46	5.260	5.550	-0.290	5.158	0.102
47	8.300	8.180	0.120	7.902	0.398
48	7.040	7.725	-0.685	7.836	-0.796
49	7.820	7.704	0.116	7.867	-0.047
50	7.590	8.041	-0.451	7.942	-0.352
51	8.300	8.054	0.246	7.848	0.452
52	7.390	6.722	0.668	7.005	0.385
53	7.050	7.119	-0.069	7.277	-0.227
54	7.520	7.566	-0.046	7.230	0.290
55	7.000	7.187	-0.187	6.974	0.026
56	7.220	7.217	0.003	7.18	0.040
Test set					
57	6.830	7.518	-0.6877	6.719	0.1111
58	5.470	5.513	-0.0433	5.243	0.2268
59	5.420	5.179	0.2413	5.268	0.152
60	5.470	5.579	-0.109	5.141	0.3287

(Continued)

Table IV *(Continued)*

Compound	pIC50	CoMFA Predict	residual (Δ)	CoMSIA Predict	residual (Δ)
61	5.460	5.166	0.2935	5.278	0.1822
62	5.450	5.922	-0.4718	5.535	-0.085
63	5.450	4.992	0.4579	5.279	0.1706
64	5.420	4.858	0.5624	5.263	0.1568
65	5.490	4.978	0.5122	5.257	0.2332
66	5.530	5.007	0.5231	5.222	0.3082
67	5.470	5.374	0.096	5.337	0.1332
68	5.520	4.946	0.5737	5.02	0.5
69	5.500	5.343	0.1571	5.032	0.4677
70	5.460	5.318	0.1416	4.913	0.5466
71	5.150	5.511	-0.3606	5.086	0.0638
72	8.300	8.123	0.1771	7.769	0.5315
73	7.920	7.792	0.128	7.952	-0.0319
74	8.520	7.823	0.6968	8.397	0.1227
75	8.100	8.099	0.0014	7.634	0.4655
76	7.300	7.777	-0.4766	7.782	-0.482
77	7.000	7.146	-0.1463	7.194	-0.1938
78	7.300	6.674	0.6262	7.167	0.1332
79	6.700	7.231	-0.5306	7.206	-0.506
80	7.300	6.843	0.4569	6.744	0.5562
81	7.400	6.567	0.8326	6.912	0.4876
82	6.520	6.944	-0.4243	6.787	-0.2668
83	6.700	7.015	-0.3154	7.229	-0.5288
84	6.860	6.708	0.1516	6.956	-0.0963
85	6.000	5.537	0.4631	5.979	0.0212
86	5.700	5.538	0.1618	6.016	-0.3159

that electrostatic regions had low correlation to biological activity and hydrogen bond donor regions and steric regions had highest correlation.

Prediction by QSAR

The predicted activity of training set and test set molecules is shown in Table IV. Figure 2 shows the prediction curves, with test set in red and training set in blue. The distribution of the test set was similar to that of training set, and hence, supporting the predictivity of our QSAR model. The 3D-QSAR models were then employed to predict the PDE-5 inhibitory activity of TCM compounds. The result of the TCM mapping is presented in Table V. The contour maps of CoMFA and CoMSIA are shown in Figures 3(a) and 3(b).

Table V
PDE-5 inhibitory activities of TCM compounds predicted by using CoMFA and CoMSIA models. Compounds that have pIC50>7 are shown here.

Compound	CoMFA pIC50	CoMSIA pIC50
1. Coixol	7.226	7.513
2. Genipin	7.352	7.378
3. Tanshinone IIB	7.474	7.191
4. Engeletin	7.398	7.131
5. Beta-sitosterol1	7.598	7.181
6. Preskimmianine	7.831	7.227
7. Sarsasa-pogenin	7.515	7.082
8. Schizandrer A	7.180	7.163
9. Gardenia jasminoides eills	7.092	7.192
10. Timospaponine1	7.063	7.631

(a) R² = 0.9478

(b) R² = 0.9474

Figure 2: Correlations between the actual pIC50 and the predicted pIC50 of the training set and the test set by (**a**) CoMFA and (**b**) CoMSIA.

(a)

(b)

(c)
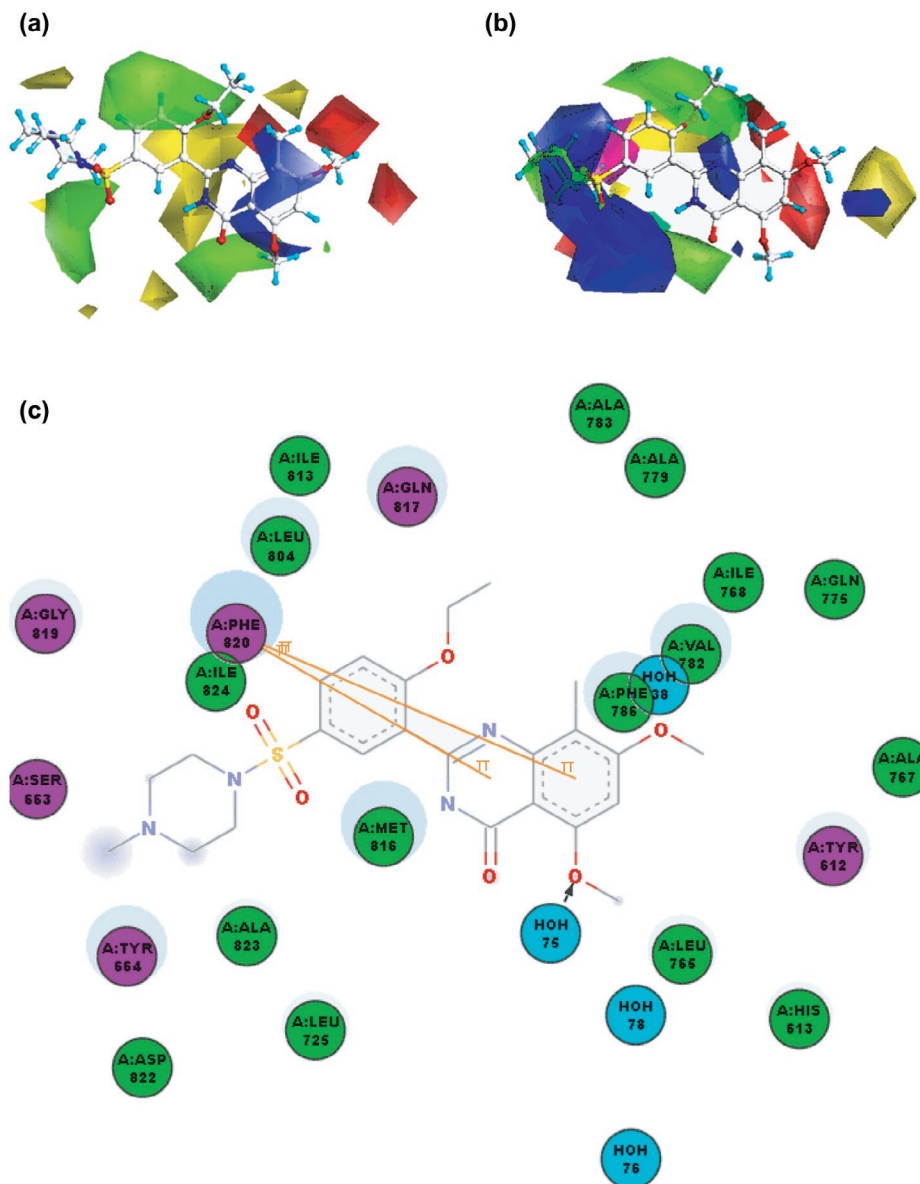
Figure 3: (**a**) CoMFA contour maps. Steric favor contributions are shown in green, and disfavor contributions are shown in yellow. Electrostatic contributions are shown in blue for electropositive favored contours and in red for electronegative favored contours. (**b**) CoMSIA contour maps. Green contours indicate steric favor contributions while yellow contours represent the opposite effect. Electropositive contours are shown in blue, and electronegative contours are shown in red. Hydrophobic favored regions are shown in purple. (**c**) Ligand interaction diagram of No. 6 from training set.

Contour Maps and Ligand Interaction Diagrams

Docking simulations were performed to analyze binding mode of ligands and to test the reliability of CoMFA and CoMSIA models. Figures 3(a) and 3(b) shows the CoMFA and CoMSIA contour maps, with compound No. 6 from the training set as reference molecule. The docking pose of compound 6 is shown in interaction diagram in Figure 3(c) (refer to Table VI for graphic element descriptions). Steric favored contours were found near R4 site (refer to Figure 1(a) for numbering system), consistent with the interaction diagram that shows a possible extension space in the binding site. Similar steric favored contributions were also found near R2 and R3 (Figures 3(a) and 3(b)), which were in agreement with the interactions observed and the binding site layout shown in Figure 3(c).

Comparing cGMP and sildenafil interaction diagrams (Figure 4), we have found several common characteristics of two ligands that cannot be readily detected from 3D-QSAR analyses: (i) presence of pi-stacking interaction to Phe820, (ii) requirement of water bridges in ligand-protein interaction, and (iii) key hydrogen bonding interaction to Gln817. As shown in Figure 4, cGMP and sildenafil share similar binding

model. Sildenafil has unreactive sulfur group instead of phosphate group of cGMP and is further stabilized with substituent.

Water molecules in the binding site were also extensive analyzed. As illustrated in Figure 5, water molecules connect ligand to protein, forming water bridges. Based on our simulation results, water molecules were essential for cGMP and sildenafil

Style Key

The following table details the definitions for the various elements in the 2D Window when displayed using the default colors and graphics:

Element	Description
(purple circle)	Residues involved in hydrogen-bond, charge or polar interactions are represented by magenta-colored circles.
(green circle)	Residues involved in van der Waals interactions are represented by green circles.
(aquamarine circle)	Water molecules are represented by aquamarine circles.
(gray circle)	Metal atoms are represented by gray circles.
(green circle with blue halo)	The solvent accessible surface of an interacting residue is represented by a blue halo around the residue. The diameter of the circle is proportional to the solvent accessible surface.
(red O atom with halo)	The solvent accessible surface of an atom is represented by a blue halo around the atom. The diameter of the circle is proportional to the solvent accessible surface.
(black dashed arrow)	Hydrogen-bond interactions with non-amino acid residues are represented by a black dashed line with an arrow head directed towards the electron donor.
(green dashed arrow)	Hydrogen-bond interactions with amino acid main chains are represented by a green dashed line with an arrow head directed towards the electron donor.
(blue dashed arrow)	Hydrogen-bond interactions with amino acid side-chains are represented by a blue dashed line with an arrow head directed towards the electron donor.
(pink double arrow)	Charge interactions are represented by a pink dashed line with arrow heads on both sides.
π σ	Pi interactions are represented by an orange line with symbols indicating the interaction.

Figure 4: Graphic elements used in the interaction diagrams. This information could be obtained from the help manual of Discovery Studio version 2.5.

to establish bonding to Tyr612 and Ala767. Using the labeling system in Figure 5, cGMP formed hydrogen bonding with H_2O^{38} and sildenafil with H_2O^{75}. Additionally, compound 5 and compound 6 from training set all had water-bridge effect similar to sildenafil binding mode (Figures 5(a), 5(b) and 6). Based on the number of water bridges, we speculate that ligand having bonding with H_2O^{38} could be more stable than having interaction with H_2O^{75}.

As for compounds from TCM database (http://tcm.cmu.edu.tw/index.php), the PDE-5 inhibitory activity was predicted by the QSAR model. The top compounds (shown in Table V) were then further filtered out via the before mentioned three binding mode characteristics. Engeletin and coixol, which satisfied these three key binding modes (shown in Figures 7 and 8) were considered as potential candidates out of the entire compound library. Coixol had the highest predicted activity but lacked of essential water bridges (Figures 5(c) and 5(d)). In this regard, engeletin could be a better a candidate than coixol. Furthermore, the water bridges formed between engeletin and PDE-5 were similar to that of cGMP.

Our results support the idea that docking study is useful in determining molecule binding mode in protein. Docking scores and scoring functions are often debated for reproducibility and reliability; however, docking simulations provide insights into binding modes that are not obtainable from normal 3D-QSAR analyses. Certain receptor-ligand interactions, such as water bridges and pi-stacking could be readily detected in docking analyses but not in 3D-QSAR. Therefore, we suggest that docking studies should be conducted for qualitative purposes rather than for quantitative purposes. According to some studies about molecular dynamics and

(a)

(b)
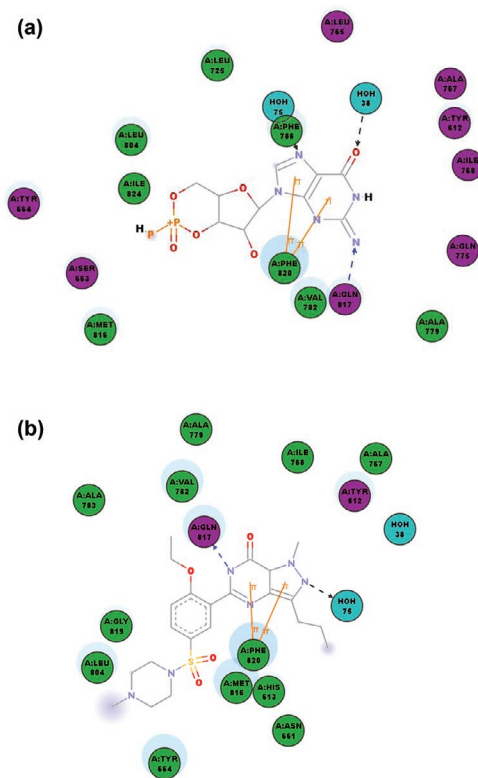
Figure 5: Ligand interaction diagrams of (**a**) cGMP and (**b**) sildenafil.
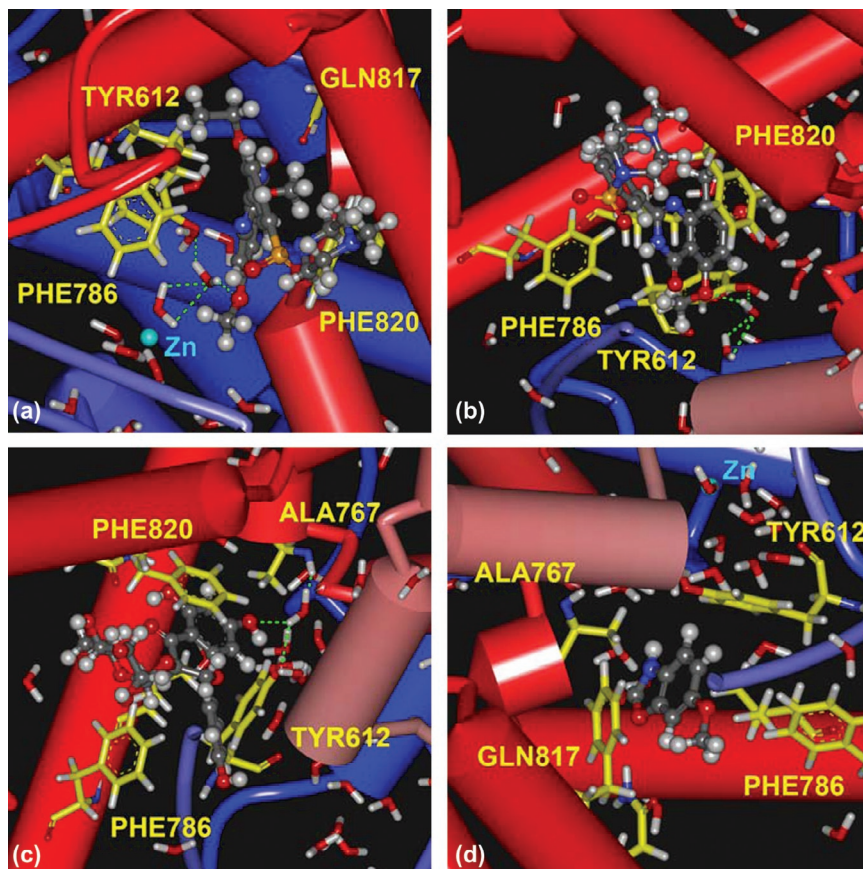
Figure 6: The docking results of (**a**) No. 5 from training set, (**b**) No. 6 from training set, (**c**) engeletin and (**d**) coixol.

molecular simulations (50-58), we will perform the molecular dynamics study to investigate this issue.

Conclusion

We have constructed predictive CoMFA and CoMSIA models, using experimentally tested PDE-5 inhibitors. Additional docking analyses of the binding mode of cGMP, sildenafil citrate and compounds from the training set have provided useful insight to the binding model of PDE-5 ligands. Overall, we have identified three PDE-5 inhibitor binding features: (i) ligand pi-stacking interaction to
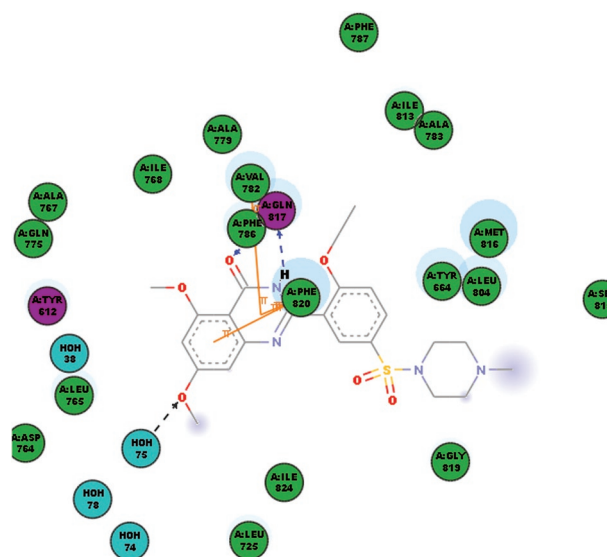
Figure 7: Ligand interaction diagram of No. 5 from training set.
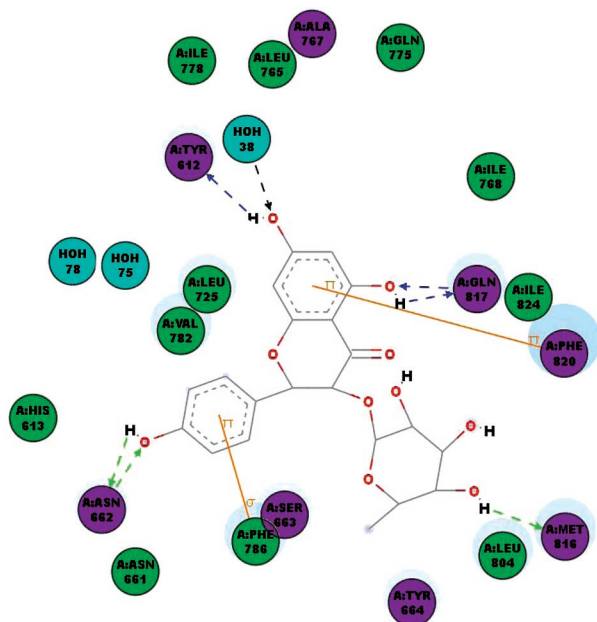
Figure 8: Ligand interaction diagram of engeletin.

Phe820, (ii) presence of water bridges that aid ligand interactions to Tyr612 and Ala767, and (iii) hydrogen bonding between ligand and Gln817.

Biological activities of compounds from our TCM database (http://tcm.cmu.edu. tw/index.php) were predicted using the predictive models and analyzed in docking simulation. Engeletin had high predicted inhibitory activity and similar water bridges as cGMP. Thus, engeletin was deemed to be the most potent PDE-5 inhibitor candidate.
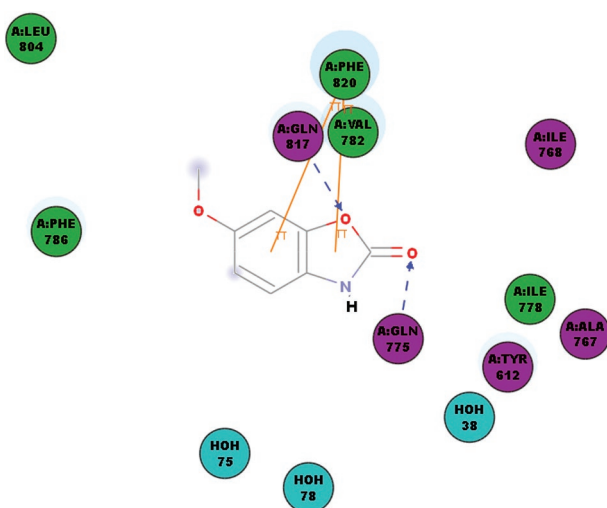
Acknowledgements

Figure 9: Ligand interaction diagram of coixol.

References

1. C. Alberti, A. Frattini, and S. Ferretti. *Minerva Urol Nefrol 45*, 49-54 (1993).
2. R. M. Rapoport and F. Murad. *J Cyclic Nucleotide Protein Phosphor Res 9*, 281-296 (1983).
3. K. Loughney, J. Taylor, and V. A. Florio. *Int J Impot Res 17*, 320-325 (2005).
4. J. A. Beavo. *Physiol Rev 75*, 725-748 (1995).
5. C. B. Johannes, A. B. Araujo, H. A. Feldman, C. A. Derby, K. P. Kleinman, and J. B. McKinlay. *J Urol 163*, 460-463 (2000).
6. S. H. Francis, T. M. Lincoln, and J. D. Corbin. *J Biol Chem 255*, 620-626 (1980).
7. S. H. Francis, I. V. Turko, and J. D. Corbin. *Prog Nucleic Acid Res Mol Biol 65*, 1-52 (2001).
8. A. L. Burnett, C. J. Lowenstein, D. S. Bredt, T. S. Chang, and S. H. Snyder. *Science 257*, 401-403 (1992).
9. A. L. Burnett. *J Androl 23*, S20-26 (2002).
10. J. L. Weeks, M. A. Blount, A. Beasley, R. Zoraghi, M. K. Thomas, K. R. Sekhar, J. D. Corbin, and S. H. Francis. *Methods Mol Biol 307*, 239-262 (2005).
11. T. Kushiro, A. Takahashi, F. Saito, Y. Otsuka, M. Soma, T. Kurihara, A. Satomura, T. Saito, and K. Kanmatsuse. *Am J Hypertens 18*, 427-430 (2005).
12. G. B. Brock, C. G. McMahon, K. K. Chen, T. Costigan, W. Shen, V. Watkins, G. Anglin, and S. Whitaker. *J Urol 168*, 1332-1336 (2002).
13. Q. Ding, L. Huo, J. Y. Yang, W. Xia, Y. Wei, Y. Liao, C. J. Chang, Y. Yang, C.C. Lai, D. F. Lee, C. J. Yen, Y. J. Chen, J. M. Hsu, H. P. Kuo, C. Y. Lin, F. J. Tsai, L.Y. Li, C. H. Tsai, and M. C. Hung. *Cancer Res 68*, 6109-6117 (2008).
14. T. N. Chang, G. J. Huang, Y. L. Ho, S. S. Huang, H. Y. Chang, and Y. S. Chang. *Am J Chin Med 37*, 797-814 (2009).
15. Y. H. Chang, J. S. Yang, J. L. Yang, C. L. Wu, S. J. Chang, K. W. Lu, J. J. Lin, T. C. Hsia, Y. T. Lin, C. C. Ho, W. G. Wood, and J. G. Chung. *Biosci Biotechnol Biochem 73*, 2589-2594 (2009).
16. L. I. D. S. Hage-Melim, C. H. T. D. P. Da Silva, E. P. Semighini, C. A. Taft, and S. V. Sampaio, *J Biomol Struct Dyn 27,* 27-35 (2009).
17. C. Arcangeli, C. Cantale, P. Galeffi, G. Gianese, R. Paparcone, and V. Rosato. *J Biomol Struct Dyn 26*, 35-47 (2008).
18. A. A. Moosavi-Movahedi, S. J. Mousavy, A. Divsalar, A. Babaahmadi, K. Karimian, A. Shafiee, M. Kamarie, N. Poursasan, B. Farzami, G. H. Riazi, G. H. Hakimelahi, F. Y. Tsai, F. Ahmad, M. Amani, and A. A. Saboury. *J Biomol Struct Dyn 27*, 319-329 (2009).
19. S. Mishra and S. Sinha. *J Biomol Struct Dyn 27*, 293-305 (2009).
20. C. Y. Chen, Y. H. Chang, D. T. Bau, H. J. Huang, F. J. Tsai, and C. H. Tsai. *Acta Pharmacol Sin 30*, 1186-1194 (2009).
21. C. Y. Chen. *J Mol Graph Model 28*, 261-269 (2009).
22. C. Y. Chen, Y. F. Chen, C. H. Wu, and H. Y. Tsai. *J Biomol Struct Dyn 26*, 57-64 (2008).
23. C. Y. Chen, Y. H. Chang, D. T. Bau, H. J. Huang, F. J. Tsai, and C. H. Tsai, C. Y. C. Chen. *J Biomol Struct Dyn 27*, 171-178 (2009).
24. Y. Guo and T. M. Wang. *J Biomol Struct Dyn 26*, 367-373 (2008).
25. Y. Houndonougbo, K. Kuczera, and G. S. Jas. *J Biomol Struct Dyn 26*, 17-34 (2008).
26. A. Mahalakshmi, K. Sujatha, and R. Shenbagarathai. *J Biomol Struct Dyn 26*, 375-385 (2008).
27. A. Cordomi, E. Ramon, P. Garriga, and J. J. Perez. *J Biomol Struct Dyn 25*, 573-587 (2008).
28. J. Wang, L. Zhao, X. Dou, and Z. Zhang. *J Biomol Struct Dyn 25*, 609-619 (2008).
29. U. B. Sonavane, S. K. Ramadugu, and R. R. Joshi. *J Biomol Struct Dyn 26*, 203-214 (2008).
30. F. Mehrnejad, and N. Chaparzadeh. *J Biomol Struct Dyn 26*, 255-262 (2008).
31. L. Zhong, and J. Xie. *J Biomol Struct Dyn 26*, 525-533 (2009).
32. J. Zhang. *J Biomol Struct Dyn 27*, 159-162 (2009).
33. M. S. Smith, S. A. Lee, and A. Rupprecht. *J Biomol Struct Dyn 27*, 105-110 (2009).
34. R. Vinekar and I. Ghosh. *J Biomol Struct Dyn 26*, 741-754 (2009).
35. E. D. Akten, S. Cansu, and P. Doruker. *J Biomol Struct Dyn 27*, 13-25 (2009).
36. A. M. Andrianov. *J Biomol Struct Dyn 26*, 445-454 (2009).
37. J. Sille and M. Remko. *J Biomol Struct Dyn 26*, 431-444 (2009).
38. G. F. Yang, H. T. Lu, Y. Xiong, and C. G. Zhan. *Bioorg Med Chem 14*, 1462-1473 (2006).
39. R. O. Hughes, J. K. Walker, J. W. Cubbage, Y. M. Fobian, D. J. Rogier, S. E. Heasley, R. M. Blevis-Bal, A. G. Benson, D. R. Owen, E. J. Jacobsen, J. N. Freskos, J. M. Molyneaux, D. L. Brown, W. C. Stallings, B. A. Acker, T. M. Maddux, M. B. Tollefson, J. M. Williams, J. B. Moon, B. V. Mischke, J. M. Rumsey, Y. Zheng, A. Macinnes, B. R. Bond, and Y. Yu. *Bioorg Med Chem Lett 19*, 4092-4096 (2009).
40. D. R. Owen, J. K. Walker, E. Jon Jacobsen, J. N. Freskos, R. O. Hughes, D. L. Brown, A. S. Bell, D. G. Brown, C. Phillips, B. V. Mischke, J. M. Molyneaux, Y. M. Fobian, S. E. Heasley, J. B. Moon, W. C. Stallings, D. Joseph Rogier, D. N. Fox, M. J. Palmer, T. Ringer, M. Rodriquez-Lens, J. W. Cubbage, R. M. Blevis-Bal, A. G. Benson, B. A. Acker, T. M. Maddux, M. B. Tollefson, B. R. Bond, A. Macinnes, and Y. Yu. *Bioorg Med Chem Lett 19*, 4088-4091 (2009).

41. H. Haning, U. Niewohner, T. Schenke, T. Lampe, A. Hillisch, and E. Bischoff. *Bioorg Med Chem Lett 15*, 3900-3907 (2005).

42. P. Srivani, E. Srinivas, R. Raghu, and G. N. Sastry. *J Mol Graph Model 26*, 378-390 (2007).

43. J. Yoo, K. M. Thai, D. K. Kim, J. Y. Lee, and H. J. Park. *Bioorg Med Chem Lett 17*, 4271-4274 (2007).

44. A. Daugan, P. Grondin, C. Ruault, A. C. Le Monnier de Gouville, H. Coste, J. M. Linget, J. Kirilovsky, F. Hyafil, and R. Labaudiniere. *J Med Chem 46*, 4533-4542 (2003).

45. A. Daugan, P. Grondin, C. Ruault, A. C. Le Monnier de Gouville, H. Coste, J. Kirilovsky, F. Hyafil, and R. Labaudiniere. *J Med Chem 46*, 4525-4532 (2003).

46. H. Duan, J. Zheng, Q. Lai, Z. Liu, G. Tian, Z. Wang, J. Li, and J. Shen. *Bioorg Med Chem Lett 19*, 2777-2779 (2009).

47. C. M. Venkatachalam, X. Jiang, T. Oldfield, and M. Waldman. *J Mol Graph Model 21*, 289-307 (2003).

48. B. J. Sung, K. Y. Hwang, Y. H. Jeon, J. I. Lee, Y. S. Heo, J. H. Kim, J. Moon, J. M. Yoon, Y. L. Hyun, E. Kim, S. J. Eum, S. Y. Park, J. O. Lee, T. G. Lee, S. Ro, and J. M. Cho. *Nature 425*, 98-102 (2003).

49. B. R. Brooks, R. E. Bruccoleri, O. B. D., S. D. J., S. S., and K. M. *J Comp Chem 4*, 187–217 (1983).

50. S. Subramaniam, A. Mohmmed, and D. Gupta. *J Biomol Struct Dyn 26*, 473-479 (2009).

51. P. N. Sunilkumar, D. G. Nair, C. Sadasivan, and M. Haridas. *J Biomol Struct Dyn 26*, 491-496 (2009).

52. H. R. Bairagya, B. P. Mukhopadhyay, and K. Sekar. *J Biomol Struct Dyn 26*, 497-507 (2009).

53. M. Parthiban, M. B. Rajasekaran, S. Ramakumar, and P. Shanmughavel. *J Biomol Struct Dyn 26*, 535-547 (2009).

54. N. A. Timofeyeva, V. V. Koval, D. G. Knorre, D. O. Zharkov, M. K. Saparbaev, A. A. Ishchenko, and O. S. Fedorova. *J Biomol Struct Dyn 26*, 637-652 (2009).

55. K. Sujatha, A. Mahalakshmi, D. K. Solaiman, and R. Shenbagarathai. *J Biomol Struct Dyn 26*, 771-779 (2009).

56. X. L. Xie, Q. S. Huang, Y. Wang, C. H. Ke, and Q. X. Chen. *J Biomol Struct Dyn 26*, 781-786 (2009).

57. G. Patargias, H. Martay, and W. B. Fischer. *J Biomol Struct Dyn 27*, 1-12 (2009).

58. C. Y. C. Chen. *J Biomol Struct Dyn 27*, 271-282 (2009).